Extreme Ultraviolet Beam Enhancement by Relativistic Surface Plasmons

G. Cantono,[1,2,3,4,*] L. Fedeli,[5] A. Sgattoni,[6,7] A. Denoeud,[1] L. Chopineau,[1] F. Réau,[1] T. Ceccotti,[1] and A. Macchi[3,4]
[1]*LIDYL, CEA, CNRS, Université Paris-Saclay, CEA Saclay, 91191 Gif-sur-Yvette, France*
[2]*Université Paris Sud, Paris, 91400 Orsay, France*
[3]*National Institute of Optics, National Research Council (CNR/INO) A. Gozzini unit, 56124 Pisa, Italy*
[4]*Enrico Fermi Department of Physics, University of Pisa, 56127 Pisa, Italy*
[5]*Department of Energy, Politecnico di Milano, 20133 Milano, Italy*
[6]*LULI-UPMC: Sorbonne Universités, CNRS, École Polytechnique, CEA, 75005 Paris, France*
[7]*LESIA, Observatoire de Paris, CNRS, UPMC: Sorbonne Universites, 92195 Meudon, France*

(Received 31 March 2018; published 28 June 2018)

The emission of high-order harmonics in the extreme ultraviolet range from the interaction of a short, intense laser pulse with a grating target is investigated experimentally. When resonantly exciting a surface plasmon, both the intensity and the highest order observed for the harmonic emission along the grating surface increase with respect to a flat target. Harmonics are obtained when a suitable density gradient is preformed at the target surface, demonstrating the possibility to manipulate the grating profile on a nanometric scale without preventing the surface plasmon excitation. In support of this, the harmonic emission is spatiotemporally correlated to the acceleration of multi-MeV electron bunches along the grating surface. Particle-in-cell simulations reproduce the experimental results and give insight on the mechanism of high harmonic generation in the presence of surface plasmons.

DOI: 10.1103/PhysRevLett.120.264803

Laser-driven high-order harmonic (HH) generation [1,2] has a strong potential in the research for bright, ultrashort sources of extreme ultraviolet (XUV) radiation, which could find applications in probing the fast dynamics of atoms and molecules [3,4] and in giving insight into the strongly nonlinear processes typical of intense laser-plasma interactions [5]. In particular, high conversion efficiencies from the infrared laser light into the XUV harmonics [6,7] are achieved when intense laser pulses ($I > 10^{18}$ W/cm^2) are focused on solid targets, where HH generation is strongly related to the collective oscillations of relativistic electrons at the sharp laser-plasma interface [8–10].

When using flat targets, both the intense laser light and the broadband XUV beam are reflected in the specular direction. On the other hand, grating targets have been investigated for the possibility to angularly separate the harmonic orders [11–16], as well as to discriminate the XUV beam from the fundamental laser frequency, whose intensity otherwise dominates the spectrum. Such a diffracting system would be beneficial for the realization of near-monochromatic sources to be applied in photoelectron spectroscopy or coherent diffraction imaging [17]. Yet, angular dispersion has the clear disadvantage of reducing the intensity of the XUV beam emitted in a specific direction.

The resonant excitation of propagating surface plasmons (SPs) on the grating surface can be explored to face this drawback [14,18]. Indeed, the periodic modulation of the grating allows satisfying the phase-matching condition between the laser pulse and the SP itself, leading to the enhancement of the electromagnetic (EM) field at the target surface. Such an enhancement is expected to boost the HH generation to higher frequencies, still profiting from the spatial separation due to diffraction. Despite the lack of a theoretical model of SPs of relativistic amplitude, the SP-driven enhancement of angularly separated HHs from grating targets has been recently observed in 2D particle-in-cell (PIC) simulations [14]. While experiments on HH generation assisted by plasmonic nanostructures have been performed only at very low laser intensities ($I \leq 10^{12}$ W/cm^2) [19–21], experimental measurements of SP-driven electron acceleration [22–24] and enhanced proton beam emission [25] have been successfully performed in the relativistic regime.

In this Letter, we study HH generation while combining the diffraction from grating targets and the EM field enhancement from SP excitation. We show that HHs emitted close to the grating surface are more intense in the presence of a SP and have a higher cutoff frequency compared to the harmonic spectrum generated by a flat target. By measuring the acceleration of energetic electrons along the grating surface [22,23], we also demonstrate that the scale length of the density gradient preformed at the target surface and required to increase the efficiency of HH generation [1,26–28] does not prevent the SP excitation, despite being of the same order of the grating depth and possibly altering the SP resonance condition. The experimental results are correlated with new PIC simulations

assessing the effect of the density gradient and a possible mechanism for the generation of the intense HHs at the grating surface.

Figure 1 illustrates the setup of the experiment performed at CEA Saclay. The 100 TW-class laser system UHI-100 delivers 25 fs pulses at a central wavelength of $\lambda \simeq 800$ nm. The energy on target is estimated close to 700 mJ within a focal spot of ~5.8 μm (FWHM), achieved with a $f/3.75$ off-axis parabola and wave front corrections performed by a deformable mirror. In these conditions, the average intensity reached $I \sim 2 \times 10^{19}$ W/cm^2 (estimated with the beam size and pulse duration at $1/e^2$). The repetition rate was limited to ~1 shot/min to proceed with the realignment of a fresh target after each shot.

We used two different targets: a 5 mm thick, flat slab of silica (F) and a grating (G30) produced by heat embossing a sinusoidal profile (with a 250 nm peak-to-valley depth) on a 23 μm thick Mylar™ foil. The phase-matching conditions predict the SP excitation when the laser pulse irradiates the grating target at the so-called resonant angle ϕ_{res}, determined by

$$\sin(\phi_{\mathrm{res}}) = \pm\sqrt{\frac{1-\omega_p^2/\omega^2}{2-\omega_p^2/\omega^2}} + j\frac{\lambda}{\Lambda}. \quad (1)$$

In this expression, valid for sharp vacuum-plasma boundaries and inferred in the linear limit of cold, collisionless plasma, ω_p and ω are, respectively, the plasma and laser frequency, j is an integer $(0, \pm 1, \ldots)$, and Λ is the grating period. For the grating used in the experiment, $\Lambda = 2\lambda$, corresponding to $\phi_{\mathrm{res}} = -30°$ for $j = 1$ and in the limit of $\omega_p \gg \omega$, where the resonant condition (1) becomes independent of the plasma density. This is consistent with previous experiments whose results were not strongly affected by the choice of the target material [22]. However, the preplasma expansion could increase ϕ_{res} as

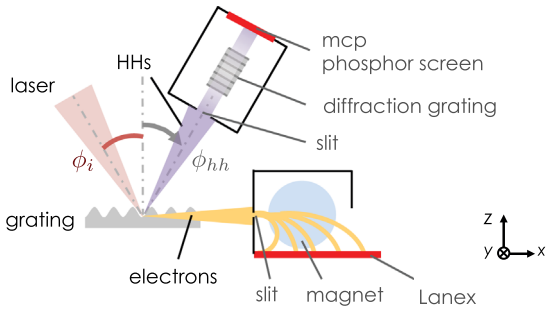

FIG. 1. Experimental setup. Angles are measured from the target normal, with the convention that $\phi_i < 0$ and the observation angle is $\phi_{hh} > 0$. For all ϕ_i, the XUV spectrometer was aligned at $-\phi_i$ (the specular, as shown), 78.5°, 82°, and 87°. HHs are spectrally dispersed by the grating along y. The electron spectrometer was placed along the grating surface. The 0.5″ mirror for the creation of the prepulse (not shown here) was placed upstream of the focusing parabola.

well as modify the dispersion relation of the SP: For these reasons, in addition to the expected ϕ_{res}, we also tested the incidence angles of −35° and −45°.

To control the formation of the preplasma, accidental ionization of the target surface was prevented by a double plasma mirror [29], which secured a temporal contrast $\geq 10^{12}$ at 5 ps before the main pulse. Then, we created the density gradient by intercepting a peripheral portion of the collimated laser beam with a small mirror and focusing it on the target before the main pulse [26]. For a given fluence, the preplasma scale length was entirely controlled by varying the delay between such a prepulse and the main pulse. The preplasma extent was then measured at a later time with the spatial-domain interferometry technique [30].

The HH emission was detected at different observation angles ϕ_{hh} by an XUV spectrometer, where the angularly resolved harmonic spectrum was spectrally dispersed by a grating and then imaged on a microchannel plate coupled to a phosphor screen. The angular acceptance was of 6° on the incidence plane (xz in Fig. 1), and the spectral range spanned between 12 and 80 nm. An electron spectrometer formed by two round magnets (0.9 T of magnetic field) and a collimating slit of 1.5 mm was aligned along the target surface to measure the energetic spectra of the SP-driven electron bunches [22,23], with a minimum detectable energy of 1.4 MeV. The detector consisted of a Lanex screen imaged by a CCD camera equipped with a 546 nm bandpass filter.

For each incidence angle ϕ_i, we looked for the highest harmonic order by varying the preplasma scale length on both the flat target (with $\phi_{hh} = -\phi_i$) and the grating (with $\phi_{hh} = 87°$). Depending on the incidence angle, the optimal scale length found for the flat target ranges from $L \sim 0.17\lambda$ (at $|\phi_i| = 30°$) to $\sim 0.12\lambda$ (at $|\phi_i| = 45°$). This order of magnitude ($\sim\lambda/10$) is consistent with recent experiments maximizing the conversion efficiency of HHs generated by the relativistic oscillating mirror mechanism (ROM) [26,31]. In addition, we found that the same values of prepulse delay optimize the HH emission also on the G30. We hence compared the hydrodynamical expansion of both targets under the fluence of the prepulse with the code ESTHER [32]. The density gradients after the same delay exhibited similar scale lengths, supporting that the HH generation with the ROM mechanism is not particularly sensitive to the target material.

Figure 2 compares the most intense harmonic spectra obtained with, respectively, the flat target irradiated at $|\phi_i| = 45°$ (with $\phi_{hh}^{\mathrm{F}} = 45°$) and the G30 irradiated at $|\phi_i| = 35°$ (with $\phi_{hh}^{\mathrm{G30}} = 87°$). In both cases, we integrated the signal of the experimental images over a ±2° angular range around ϕ_{hh}. The spectrum from the flat target displays HHs above the noise level until the maximum harmonic order $m_{\mathrm{max}}^{\mathrm{F}} \sim 27$, whereas the G30 exhibits a distinct emission up to $m_{\mathrm{max}}^{\mathrm{G30}} \sim 40$. Moreover, the intensity of a selection of harmonic orders can be equivalent to (from

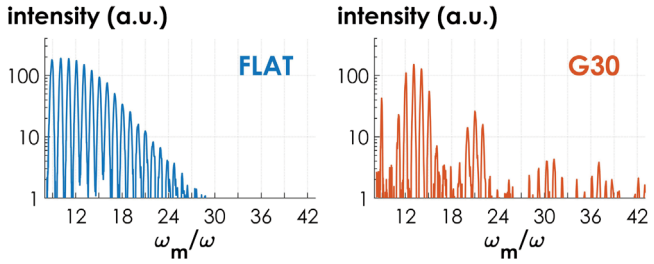

FIG. 2. Single-shot harmonic spectra from the flat target ($|\phi_i| = 45°$, $\phi_{hh} = 45°$) and the G30 ($|\phi_i| = 35°$, $\phi_{hh} = 87°$) at the optimal preplasma scale length. The spectrum from the G30 reaches $m_{max} \sim 40$, and the intensity of some harmonic orders is as high as (m from 12 to 15) or higher than (m from 18 to 21) with the flat target; the modulated intensity is caused by diffraction, for which only the HHs that fulfill the grating equation are emitted along the chosen ϕ_{hh}.

$m = 12$ to $m = 15$) or even higher than (from $m = 18$ to $m = 21$) the intensity of the same HHs emitted from the flat target. Both these observations suggest that the grating displays enhanced HH generation. We ascribe this effect to the excitation of a SP at $|\phi_i| = 35°$ instead of ϕ_{res}, attributing the resonance shift to the preplasma formation.

Further support for the SP excitation comes from the fact that, although the well-known grating equation predicts the emission of HHs near the target surface also for different values of ϕ_i, broad and intense harmonic spectra are observed only when the G30 is irradiated at $\phi_i = -35°$. To illustrate this, Fig. 3 summarizes the harmonic emission for all the investigated incidence angles, by plotting m_{max} as a function of the observation angle. The maximum order was here defined as the last order in each harmonic spectrum where the signal was still 5 times the background level. The emission from F in the specular direction and from G30 along various ϕ_{hh} are indicated with, respectively, empty and filled areas. For both targets, the HHs in the specular direction increase with the incidence angle, following the increment of the electric field component along the plasma normal [1]. However, the G30 exhibits higher harmonic orders in the tangent direction, with a dramatic enhancement when $\phi_i = -35°$.

A preplasma-induced modification of the SP resonant angle in Eq. (1) is also supported by the measurements of the electron acceleration. Figure 4(a) shows the maximum energy of the electrons accelerated along the grating surface as a function of the gradient scale length and for all the incidence angles. We defined the maximum energy in the electronic spectra recorded by the Lanex screen when the signal was twice the noise level. With a steep density gradient ($L = 0$), the G30 emits energetic electrons when irradiated at the expected resonant angle $\phi_{res} = -30°$, in agreement with the recent measurements of SP-driven electron acceleration [22]. But for the gradient scale lengths that optimize the HH generation ($0.1\lambda < L < 0.2\lambda$), the electron acceleration is efficient only at $\phi_i = -35°$, which also corresponds to the incidence angle where the highest frequencies in the harmonic spectrum were observed. As the SP amplitude and consequently the electron energy are expected to scale with the plasma density [23,33], the preplasma formation can also explain the lower energy (~10 MeV) observed in this case. In any case, the electrons emitted for $\phi_i = -30°$ and $L \neq 0$ are far slower, with energies comparable as for the nonresonant angle (−45°).

A similar shift of the resonant angle is also found in PIC simulations. We used the open source PIC code PICCANTE [34] to perform 2D simulations of both harmonic and electron emission from a G30 irradiated at various incidence angles in the presence of a density gradient. We modeled a 2λ thick overdense target, with an initial density of $n_0 = 100n_c$

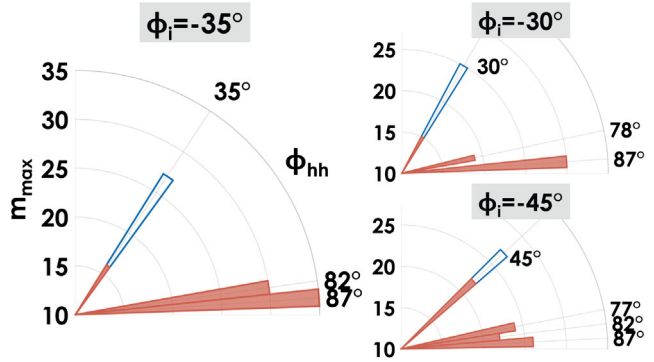

FIG. 3. Maximum harmonic order emitted by the G30 (red, filled areas) and the F (blue, empty areas) along various observation and incidence angles. As in Fig. 1, the laser beam comes from the left ($\phi_i < 0$). The values in the histograms represent m_{max} as resulting from the average of N laser shots ($N \geq 5$) acquired with the same ϕ_i and ϕ_{hh}; the standard error on m_{max} is around 1. A clear increase of m_{max} is observed in the tangent direction for $|\phi_i| = 35°$.

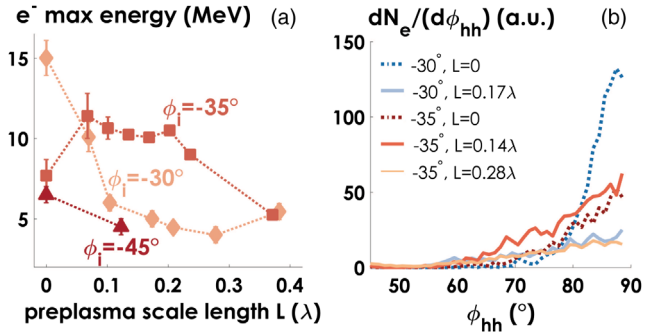

FIG. 4. (a) Maximum energy of electrons emitted along the surface of the G30, as a function of the gradient scale length and of the incidence angle (average over N shots, $N \geq 5$). Energetic electrons are produced at either $|\phi_i| = 30°$ or 35° depending on the preplasma extent, supporting a shift of the resonant angle. (b) Electron spatial distribution from 2D PIC simulations, for different combinations of ϕ_i and preplasmas. At the optimal scale length, the highest electron flux is obtained for $|\phi_i| = 35°$.

(n_c is the critical density at the laser wavelength, defined as $n_c = 1.1 \times 10^{21} \lambda_{[\mu m]}^{-2}$ cm^{-3}) and an exponential density ramp along the target normal, characterized by the same scale lengths as in the experiment. The EM field of the laser pulse had a Gaussian transverse profile with a waist of 5λ, a $\cos^2$ temporal profile with $12\lambda/c$ duration (FWHM), P polarization, and a peak normalized amplitude of $a_0 = 0.85(10^{-18} I_{[W/cm^2]} \lambda_{[\mu m]}^2)^{1/2} = 5$, corresponding to an average intensity of $\sim 3 \times 10^{19}$ W/cm^2. We used a box size of $60\lambda \times 60\lambda$ with 100 electrons and 36 ions per cell. The spatial resolution was $\lambda/335$ in each direction so as to resolve the HHs with at least 10 points per oscillation until $m = 34$. To limit the computational load, we looked at the harmonic emission at $t = 35\lambda/c$, i.e., when the laser pulse has been entirely reflected by the plasma and we expect the HH generation to have fully occurred. However, the electron acceleration along the surface develops on longer times, so for the electron detection we extended the simulations until $t = 55\lambda/c$ with a box of $100\lambda \times 100\lambda$, reducing the spatial resolution to $\lambda/100$ and $\lambda/60$ over x and y, respectively.

Figure 4(b) shows the spatial distributions of electrons above 10 MeV of energy accelerated along the grating surface for different incidence angles and preplasma extents. With the unperturbed G30 ($L = 0$), the electron emission is most prominent at resonance ($|\phi_i| = |\phi_{res}| = 30°$) [22]. But as soon as the preplasma is added, the emission at resonance drops dramatically, and the energetic electrons are accelerated for $|\phi_i| = 35°$, in agreement with the experimental results. Also, exceeding the optimal scale length smooths out the grating profile and prevents electron acceleration.

The role of the density gradient in increasing the harmonic yield clearly emerges from the simulated harmonic spectra illustrated in Fig. 5 for a G30. In this case, the intensity was calculated by integrating the Fourier transform of the magnetic energy density $\propto |B_z|^2$ of each harmonic order along the preferred ϕ_{hh}. For both incidence angles, the density gradient leads to more intense harmonic spectra, with a gain factor of ~ 5 at high m (~ 40). The signal at $|\phi_i| = 35°$, in particular, is also modulated because of diffraction as in the experimental results, with the highest enhancement obtained on the harmonic orders from 10 to 13 and around 20.

Finally, the PIC simulations allowed us to compare the trajectories of some test electrons with the HH generation at the grating surface, aiming to explain why the intense XUV beams are observed especially in the tangent direction. The result, which is detailed in a movie in Supplemental Material [35], shows a distinct spatial correlation between the harmonic bursts and bunches of energetic electrons that are accelerated in the region of the focal spot. This suggests that the EM field of the laser pulse is scattered by the electrons accelerated along the surface by the SP, and the emitted radiation is the more collimated in the tangent direction the more energetic the electrons become. This

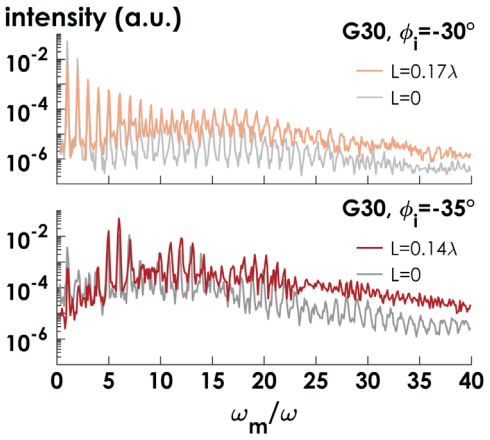

FIG. 5. Intensity profiles of the harmonic spectra integrated over $82° < \phi_{hh} < 87°$ for the G30. Colored (gray) lines represent the results of the PIC simulations with (without) the exponential density gradient at the target surface. The preplasma enhances HH generation in both configurations.

mechanism for HH generation has indeed some analogies with the operation of a free electron laser [36], where in our case the accelerator is the SP and the undulator is the laser field near the grating surface; also, the periodic modulation of the latter is imprinted in the field pattern, generating the spatial diffraction of the emitted radiation. At the same time, the observed electron bunching along the velocity direction can contribute to enhancing the intensity of the scattered radiation. We also point out that, although this mechanism is particularly efficient in the presence of a SP, this picture allows for the emission of grazing HHs also with flat targets, where the electron acceleration along the surface derives from the momentum conservation of the oblique incident laser light. As a matter of fact, HHs generated close to the surface of flat targets are also visible in PIC simulations [14].

In conclusion, we reported the first experimental observation of a SP-driven enhancement of HH generation from grating targets irradiated at relativistic intensities. Our results demonstrate that the SP excitation partly counteracts the intensity loss of the HHs dispersed by the grating, increasing the generation efficiency of some harmonic orders while preserving the angular separation from the fundamental laser frequency. The harmonic enhancement is particularly efficient along the grating surface, where the laser radiation is scattered by bunches of energetic electrons accelerated by the SP. The electron acceleration itself also proves that plasmonic effects are still accessible at relativistic intensities also in the presence of the controlled density gradients that are required to achieve efficient HH generation.

Future optimization of our results with solid blazed gratings [12], at an increased repetition rate [37], or with grating modulations produced by fully optical techniques [38] may lead to the development of a bright source of

XUV beams overlapped and synchronized with the acceleration of high-charge, multi-MeV electron bunches.

We acknowledge M. Květoň (HoloPlus, Prague, Czech Republic) for the grating manufacturing and the computational support from HPC Cluster CNAF (Bologna, Italy), with the precious assistance of S. Sinigardi. The research received financial support from Université Franco-Italienne (Vinci program 2015, Grant No. C2-92) and from Agence Nationale pour la Recherche (Grant No. ANR-14-CE32-0011).

*giada.cantono@fysik.lth.se

[1] C. Thaury and F. Quéré, J. Phys. B **43**, 213001 (2010).
[2] U. Teubner and P. Gibbon, Rev. Mod. Phys. **81**, 445 (2009).
[3] G. D. Tsakiris, K. Eidmann, J. Meyer-ter Vehn, and F. Krausz, New J. Phys. **8**, 19 (2006).
[4] T. Pfeifer, C. Spielmann, and G. Gerber, Rep. Prog. Phys. **69**, 443 (2006).
[5] A. Leblanc, S. Monchocé, C. Bourassin-Bouchet, S. Kahaly, and F. Quéré, Nat. Phys. **12**, 301 (2016).
[6] B. Dromey, M. Zepf, A. Gopal, K. Lancaster, M. S. Wei, K. Krushelnick, M. Tatarakis, N. Vakakis, S. Moustaizis, R. Kodama, M. Tampo, C. Stoeckl, R. Clarke, H. Habara, D. Neely, S. Karsch, and P. Norreys, Nat. Phys. **2**, 456 (2006).
[7] D. an der Brügge and A. Pukhov, Phys. Plasmas **17**, 033110 (2010).
[8] R. Lichters, J. Meyer-ter Vehn, and A. Pukhov, Phys. Plasmas **3**, 3425 (1996).
[9] T. Baeva, S. Gordienko, and A. Pukhov, Phys. Rev. E **74**, 065401 (2006).
[10] D. an der Brügge, N. Kumar, A. Pukhov, and C. Rödel, Phys. Rev. Lett. **108**, 125002 (2012).
[11] X. Lavocat-Dubuis and J.-P. P. Matte, Phys. Plasmas **17**, 093105 (2010).
[12] M. Yeung, B. Dromey, C. Rödel, J. Bierbach, M. Wünsche, G. Paulus, T. Hahn, D. Hemmers, C. Stelzmann, G. Pretzler, and M. Zepf, New J. Phys. **15**, 025042 (2013).
[13] M. Cerchez, A. L. Giesecke, C. Peth, M. Toncian, B. Albertazzi, J. Fuchs, O. Willi, and T. Toncian, Phys. Rev. Lett. **110**, 065003 (2013).
[14] L. Fedeli, A. Sgattoni, G. Cantono, and A. Macchi, Appl. Phys. Lett. **110**, 051103 (2017).
[15] S. J. Zhang, H. B. Zhuo, D. B. Zou, L. F. Gan, H. Y. Zhou, X. Z. Li, M. Y. Yu, and W. Yu, Phys. Rev. E **93**, 053206 (2016).
[16] G. Zhang, M. Chen, F. Liu, X. Yuan, S. Weng, J. Zheng, Y. Ma, F. Shao, Z. Sheng, and J. Zhang, Opt. Express **25**, 23567 (2017).
[17] R. L. Sandberg, A. Paul, D. A. Raymondson, S. Hädrich, D. M. Gaudiosi, J. Holtsnider, R. I. Tobey, O. Cohen, M. M. Murnane, H. C. Kapteyn, C. Song, J. Miao, Y. Liu, and F. Salmassi, Phys. Rev. Lett. **99**, 098103 (2007).
[18] A. Macchi, Phys. Plasmas **25**, 031906 (2018).
[19] I.-Y. Park, S. S.-W. S. Kim, J. Choi, D.-H. Lee, Y.-J. Kim, M. F. Kling, M. I. Stockman, and S. S.-W. S. Kim, Nat. Photonics **5**, 677 (2011).
[20] M. Sivis, M. Duwe, B. Abel, and C. Ropers, Nat. Phys. **9**, 304 (2013).
[21] S. Han, H. Kim, Y.-J. Y. W. Kim, Y.-J. Y. W. Kim, S. S.-W. S. Kim, I.-Y. Park, and S. S.-W. S. Kim, Nat. Commun. **7**, 13105 (2016).
[22] G. Cantono, A. Sgattoni, L. Fedeli, D. Garzella, F. Réau, C. Riconda, A. Macchi, and T. Ceccotti, Phys. Plasmas **25**, 031907 (2018).
[23] L. Fedeli, A. Sgattoni, G. Cantono, D. Garzella, F. Réau, I. Prencipe, M. Passoni, M. Raynaud, M. Květoň, J. Proska, A. Macchi, and T. Ceccotti, Phys. Rev. Lett. **116**, 015001 (2016).
[24] A. Sgattoni, L. Fedeli, G. Cantono, T. Ceccotti, and A. Macchi, Plasma Phys. Controlled Fusion **58**, 014004 (2016).
[25] T. Ceccotti *et al.*, Phys. Rev. Lett. **111**, 185001 (2013).
[26] S. Kahaly, S. Monchocé, H. Vincenti, T. Dzelzainis, B. Dromey, M. Zepf, P. Martin, and F. Quéré, Phys. Rev. Lett. **110**, 175001 (2013).
[27] C. Rödel *et al.*, Phys. Rev. Lett. **109**, 125002 (2012).
[28] A. Tarasevitch, K. Lobov, C. Wünsche, and D. von der Linde, Phys. Rev. Lett. **98**, 103902 (2007).
[29] C. Thaury, F. Quéré, J.-P. Geindre, A. Levy, T. Ceccotti, P. Monot, M. Bougeard, F. Réau, P. D'Oliveira, P. Audebert, R. Marjoribanks, and P. Martin, Nat. Phys. **3**, 424 (2007).
[30] M. Bocoum, F. Böhle, A. Vernier, A. Jullien, J. Faure, and R. Lopez-Martens, Opt. Lett. **40**, 3009 (2015).
[31] A. Leblanc, Ph.D. thesis, Université Paris-Saclay, 2016.
[32] J. P. Colombier, P. Combis, A. Rosenfeld, I. V. Hertel, E. Audouard, and R. Stoian, Phys. Rev. B **74**, 224106 (2006).
[33] C. Riconda, M. Raynaud, T. Vialis, and M. Grech, Phys. Plasmas **22**, 073103 (2015).
[34] A. Sgattoni, L. Fedeli, S. Sinigardi, A. Marocchino, A. Macchi, V. Weinberg, and A. Karmakar, arXiv:1503.02464.
[35] See Supplemental Material at http://link.aps.org/supplemental/10.1103/PhysRevLett.120.264803 for movies showing the harmonic emission overlapped with the acceleration of electron nanobunches at the grating surface. A description of the simulation parameters for the two presented configurations of preplasma and incidence angle is included.
[36] C. Pellegrini, A. Marinelli, and S. Reiche, Rev. Mod. Phys. **88**, 015006 (2016).
[37] A. Borot, A. Malvache, X. Chen, D. Douillet, G. Iaquianiello, T. Lefrou, P. Audebert, J.-P. Geindre, G. Mourou, F. Quéré, and R. Lopez-Martens, Opt. Lett. **36**, 1461 (2011).
[38] S. Monchocé, S. Kahaly, A. Leblanc, L. Videau, P. Combis, F. Réau, D. Garzella, P. D'Oliveira, P. Martin, and F. Quéré, Phys. Rev. Lett. **112**, 145008 (2014).